IEEE Access
Multidisciplinary | Rapid Review | Open Access Journal

Received July 15, 2019, accepted July 23, 2019, date of publication August 13, 2019, date of current version August 28, 2019.

Digital Object Identifier 10.1109/ACCESS.2019.2935103

Adaptive Fuzzy Control Strategy for a Single-Wheel Transportation Vehicle

CHIH-HUI CHIU
Department of Communications, Navigation, and Control Engineering, National Taiwan Ocean University, Keelung City 20224, Taiwan
e-mail: chchiu@ntou.edu.tw

ABSTRACT A novel model free adaptive Mamdani-like fuzzy controller (AMLFC) is adopted for a single-wheel transportation vehicle (SWTV) control problem in this study. A single-wheel transportation vehicle is designed and implemented. Single-wheel vehicles are simple in their mechanical frames. A single-wheel vehicle consists of a U-shaped platform, a wide wheel, and a DC motor with gearbox. A control technique for use by a person riding on an SWTV that enables real-world control of electric unicycles with unknown system external disturbances is proposed. Such an SWTV can move around stably. Moreover, an SWTV can also stand up in a fixed-point self-balance without touching the ground when a person rides on it. AMLFC is a modification of the usual Mamdani-like fuzzy controller. The main purpose of this study is to adopt an automatic balance control scheme for an electric unicycle motion control. Because the system model of the electric unicycle is time varying and nonlinear, an adaptive fuzzy control strategy with no system information is proposed. The AMLFC variables, including the mean and variance of membership functions, are tuned in real time based on the dynamic gradient descent method. Moreover, the learning rates of the parameter adaptive laws are decided by using the Lyapunov analytical method, which makes system error convergence. Therefore, it shows dynamic mapping and has good control performance compared with the existing Mamdani-like fuzzy controller. In addition, an SWTV based on a microcontroller with some handmade hardware circuits is implemented. Finally, the availability of the proposed novel adaptive Mamdani-like fuzzy controller is proven by the real-time application of SWTVs.

INDEX TERMS Electric unicycle, adaptive fuzzy control, microcontroller.

I. INTRODUCTION

Modern control systems are characterized by fast and precise motion, which is achieved by rotating motors with mechanical structures. These mechanical structures not only significantly decrease the system speed and system performance but also produce friction and vibration. In some applications, simplification in actuation systems is a popular research topic. System actuation simplification may primarily reduce the system cost, energy consumption, mechanical structure design and system uncertainty. An underactuated system is defined as a number of actuators less than the degrees of freedom of the system. Underactuated systems can be found in many control applications, such as biped robots, helicopters and inverted pendulums. For some applications, underactuated systems may be designed to efficiently suffer the breakdown of the actuators.

The associate editor coordinating the review of this article and approving it for publication was Tao Wang.

Many reports in the literature involve the study of the system control of inverted pendulums. The inverted pendulum is an example of an underactuated and highly unstable system. The main purpose of this work is to balance the pendulum while the pendulum is standing upright. Recently, there have been numerous extensions to the control system of a traditional inverted pendulum. One of the most challenging tasks is to control the inverted pendulum system when the trolley is not on a fixed track. Clearly, the development of the controller becomes more and more difficult because of the physical structure. Mobile robot research has received much attention. Specifically, many research studies are conducted on wheeled robot control.

In [1], the authors presented an efficient control method for a wheeled inverted pendulum control. The proposed method consists of model predictive control and an adaptive robust scheme. In [2], a rotary inverted pendulum system control problem was proposed. The authors dealt with the swing-up and stability problem using novel control approaches. In [3],

the authors proposed a method to deal with the stability for an inverted cart-pendulum system control. The author presented a novel proportional–integral–derivative controller for a two-wheeled inverted pendulum position control in [4]. In [5], the author presented an observer-based controller for cart inverted pendulum control.

On the control view, intelligent control theories (e.g., genetic algorithm, neural network control, fuzzy logic control, or cerebellar model articulation controller) [6]–[11] provide a design method that is different from the traditional control method. They give a manner for designing a real-time controller of an unknown or uncertain system in the last years. Many scholars believe that neural networks (NNs) can provide an effective strategy for the control of complex nonlinear systems when the system model does not exist. Unfortunately, in NNs, because of the need to update all the system parameters in each learning cycle, the learning is slow. Consequently, the control performance of NNs will be limited to a system that needs to learn online. Recently, the cerebellar model articulation controller (CMAC) has been used in many control system applications. In general, the main advantages of CMAC are that it has a fast learning speed, simple calculations, good generalization ability and easy realization of the controller. Nevertheless, the static network characteristic of CMAC is the major disadvantage.

Over the past ten years, the fuzzy control method has been widely used in nonlinear systems control without system information. Fuzzy logic control technology always applies the people experience to real-time control applications. The fuzzy control method is widely used in complex control applications due to its easy realization and simple calculation [12]–[14]. Nevertheless, fuzzy rules and membership functions are usually designed by users using a trial and error procedure. Moreover, the suitable parameters of a fuzzy controller are always determined based on the experience of the designers, as is the case for the Mamdani-type fuzzy control technique. Clearly, this determination will introduce many difficulties for real-world control via fuzzy control technology. Furthermore, a clear technical approach for fuzzy controller design is also the lack of achieving the accepted control performance. Even though the fuzzy logic control method is used in many domains, the fuzzy control technique is not frequently used in eventful applications because the analysis techniques for fuzzy controller design have not been very well developed.

In this work, the design and implementation of an electric unicycle control system was carried out. Such a platform is moved by a single wheel and is different from multiwheel platforms. Using such a mechanical frame, the unicycle control is more difficult to achieve than the control of a multi-wheel structure. Clearly, such a system is highly nonlinear. Real-time control systems typically use motors and gearboxes to realize the system motion control. An electric unicycle is composed of a chassis, one wide wheel, six batteries, one motor and control circuits. There are many nonlinear parts in this system. Consequently, the mathematical model of the unicycle may be inaccurate and complicated. Notably, traditional control methods always require an exact system dynamic model. Because an electric unicycle is highly nonlinear, it is arduous to control an electric unicycle using traditional control techniques.

In this study, a single-wheel transportation vehicle (SWTV) was designed and implemented. The drive device consists of gearboxes and a DC servo motor with an encoder. Sensors such as an inclinometer and a gyroscope are also placed on the chassis. Its weight is approximately 30 kg. The height of the unicycle is approximately 40 cm. A C8051F120 development kit that is composed of various hardware components is the system control core. SWTV control is realized based on a novel adaptive Mamdani-like fuzzy controller (AMLFC). The major drawback of a traditional Mamdani-like fuzzy controller is that these controllers are designed for static networks. However, this AMLFC is an improved type of the usual fuzzy control algorithm because the membership function variables are self-adjustment online via proposed adaptive laws capturing system dynamics. Because the AMLFC can capture the system response under dynamic conditions, the controller has good performance for systems without model information rather than the traditional fuzzy control system. Furthermore, to guarantee the convergence of system error, the AMLFC learning rates are decided according to a systematic algorithm based on the Lyapunov method. This is a novel approach. Finally, the effectiveness of the AMLFC is confirmed by the practical application of SWTVs.

II. SINGLE-WHEEL TRANSPORTATION VEHICLE

Figure 1 shows a simple diagram of the SWTV.

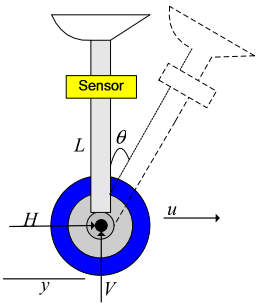

FIGURE 1. Simple diagram of the SWTV.

Single-wheel vehicles are simple in their mechanical frames. A single-wheel vehicle consists of a U-shaped platform, a wide wheel, and a DC motor with gearbox. Fig. 1 shows the structure of a single-wheel vehicle system with two degrees of freedom. In Fig. 1, θ is the angle of the SWTV, L is the length of the body of the SWTV, H is the force on the unicycle horizontal axis, V is the force on the unicycle vertical axis, u is the force applied on the electric unicycle, and y is the moving distance of the vehicle. This nonlinear system dynamics of two degrees of freedom needs to be fully

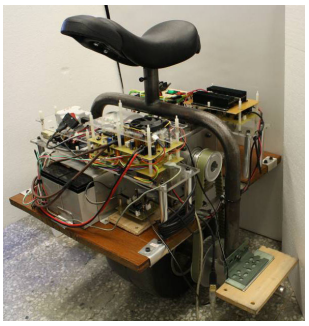

FIGURE 2. Single-wheel transportation vehicle.

described by four state variables. Clearly, the electric unicycle is a complicated platform.

Fig. 2 shows the configuration of the electric unicycle experimental system. The vehicle is composed of one 18.5-inch tire, one motor, batteries, one motor driver circuit, filter circuits, one gyroscope sensor, one tilt sensor, and a C8051F120 development kit (C8051F120DK) (Silicon Laboratories, ''C8051F12x Mixed Signal ISP Flash MCU Family'' 2005). The motor driver circuit is used to send a control signal to drive the motor. The angle and the angular velocity of vehicle body inclination are measured using sensors. To maintain the vehicle body in the upright position, the C8051F120DK receives the signals from the sensors and sends suitable commands to the motor driver circuit.

The adaptive Mamdani-like fuzzy control algorithms are accomplished in the C8051F120DK unit, which is produced by Silicon Laboratories. C8051F120DK is a mixed-signal system-on-a-chip microcontroller unit. C8051F120DK has 128 kilobytes of read-only memory (ROM), 64 kilobytes of random access memory (RAM), eight 12-bit/8-bit analog-to-digital converters (ADCs), two 8-bit digital-to-analog converters (DACs), eight bidirectional and bit-addressable input/output (I/O) ports, two universal asynchronous receiver/transmitter port, a system management bus, a serial peripheral interface (SPI), five programmable 16-bit timers/counters for general purposes and six programmable counter arrays (PCAs) for pulse width modulation. In the system, the working clock of the system is 100 MHz. The C8051F120DK is used to capture the analog measurement signals, including the body angle and the angular velocity, via its built-in 12-bit ADC interface. Moreover, C8051F120DK has pipelined instruction architecture with 70% of the instruction set executing in 1 or 2 system clocks. Next, the C8051F120DK uses the above-described information to calculate the desired commands of the DC motor to drive the vehicle platform. Fig. 3 is the C8051F120DK family block diagram.

Moreover, some external handmade circuits are combined to convert the commands to feed into the motor driver to control the built system in a suitable manner. One H-bridge circuit is designed to drive motor. This system is driven using a pulse-width modulation (PWM) square

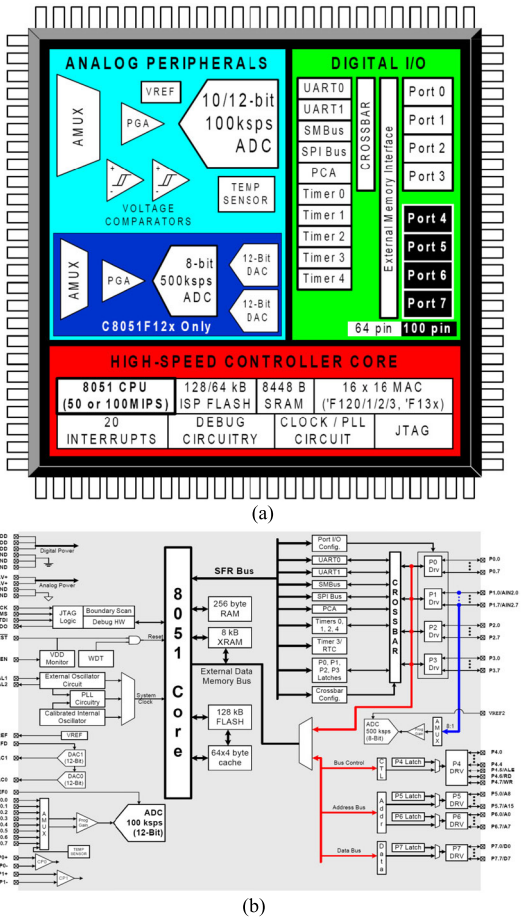

FIGURE 3. (a) High-speed mixed-signal ISP FLASH MCU family. (b) The C8051F120DK block diagram (Silicon Laboratories, "C8051F12x mixed signal ISP Flash MCU Family" 2005).

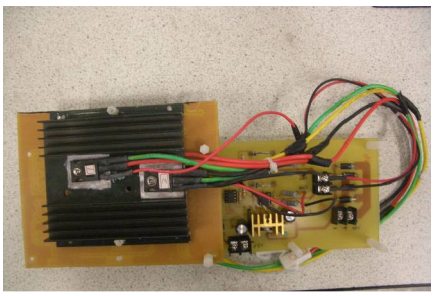

FIGURE 4. Motor drive circuit.

wave (0–24 V, 10kHz). Fig. 4 is the motor drive circuit. Signals from sensors are obtained by a sensor and filter circuit. Moreover, the system noise signals are also filtered out by the sensor and the filter circuit. Fig. 5 is a fourth-order Butterworth low-pass filter used in this work. Fig. 6 is a comparison of the signal before and after processing through the low-pass filter. Analog-to-digital converters are used to convert the system analog information to digital signals.

Algorithm1 denotes the C8051F120DK code to obtain system information including the rate of change of the angle and

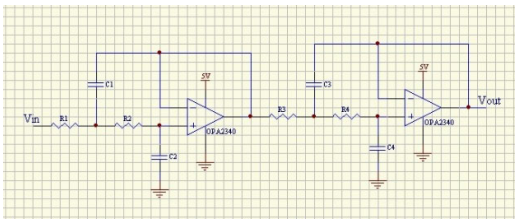

FIGURE 5. Fourth-order butterworth low-pass filter.

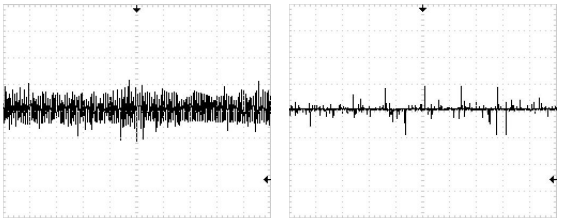

FIGURE 6. (a) Signal before processing through the low-pass filter. (b) Signal after processing through the low-pass filter.

Algorithm 1 Get the Posture of the System

Parameter setting: The value of incline meter ***Tile***, the value of gyroscope ***Gyro***

C Code:

```
for (count_c=0; count_c<AT; count_c++)
    {
        MAX197_CT();
        for (a=0; a<2; a++)
            {
    Sample[a][0]+ =AData[a][0];
            }
Delay_X1us(1);
    }
for (a=0; a<2; a++)
    {
        AData[a][0]=(Sample[a][0]/AT);
        Sample[a][0]=0;
    }
Tilt=AData[0][0];
Gyro=AData[1][0];
```

End Algorithm

angle. Algorithm2 is the C8051F120DK code to send PWM to drive motors.

In this work, the transportation vehicle system has a base carrying a 24-V dc motor with gears for the rotating wheel. Fig. 7 shows the vehicle platform. The motor is mounted on a platform. Therefore, the system can move along a straight line. The control system is connected to the control board, C8051F120DK, by the handmade circuits, the motor driver circuits, and the filter circuits and sensors required to measure the platform status. The SWTV is approximately 40-centimeters high. Fig. 8 shows the C8051F120DK unit and the handmade circuits.

Algorithm 2 PWM Output for the DC Motor

Parameter setting: The output of the fuzzy control algorithm ***PWM***

C Code:

```
char SFRPAGE_save = SFRPAGE;
        if (PWM>100)
            PWM=100;
        if (PWM<0)
            PWM=0;
SFRPAGE = PCA0_PAGE;
PCA0CPH0=PWM*2.55;
output=PCA0CPH0;
SFRPAGE = SFRPAGE_save;
```

End Algorithm

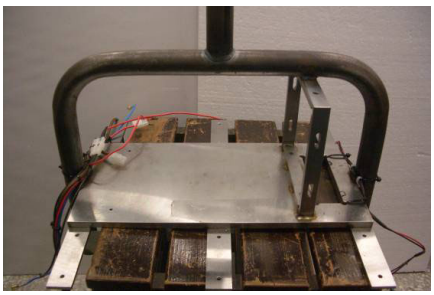

FIGURE 7. Vehicle platform.

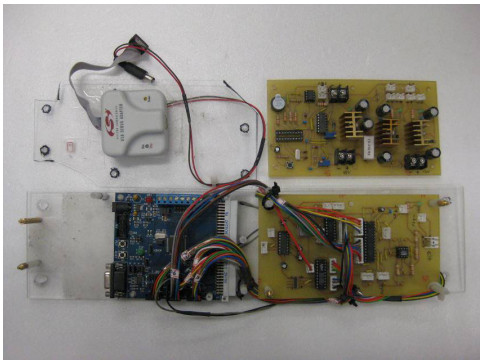

FIGURE 8. The C8051F120DK unit and the handmade circuits.

III. ADAPTIVE FUZZY CONTROLLER

A. MAMDANI TYPE FUZZY CONTROL

At the beginning of this section, the operation mechanism of the traditional fuzzy system will be reviewed. The output of the fuzzy system is u and the inputs are $x_i, i = 1, \ldots, n$, where n is the dimension of the input of the fuzzy system. Next, the entire number of fuzzy rules in the fuzzy system is m. The fuzzy rule can be expressed as follows:

$$R^j: \text{ If } x_1 \text{ is } A_1^j, \ldots, \text{ and } x_n \text{ is } A_n^j, \quad \text{then } u_j \text{ is } B_j \qquad (1)$$

In the fuzzy mechanism, the crisp input universe set is divided into fuzzy sets $A_1^j, \ldots, A_n^j$, and the outputs u_j and B_j and $j = 1, \ldots, m$ are fuzzy singletons.

The Gaussian function, which is utilized as the antecedent part of the fuzzy mechanism, can be represented as

$$A_i^j = \exp\left[\frac{-(x_i - m_{ij})^2}{v_{ij}^2}\right], \tag{2}$$

where A_i^j is the jth fuzzy rule of the ith input variable. m_{ij} and v_{ij} are the mean and variance of A_i^j, respectively. Thus, the consequent part of the fuzzy mechanism is

$$B_j = \begin{cases} 1, & u_j \text{ equals an assigned value} \\ 0, & \text{others} \end{cases} \tag{3}$$

Moreover, the fuzzy defuzzification mechanism is the center of gravity method. The crisp output u is derived as

$$U = \frac{\sum_{j=1}^{m} u_j \prod_{i=1}^{n} A_i^j(x_i)}{\sum_{j=1}^{m} \prod_{i=1}^{n} A_i^j(x_i)} = \frac{\Theta^{\mathrm{T}}\Gamma}{\sum_{j=1}^{m} \prod_{i=1}^{n} A_i^j(x_i)}, \tag{4}$$

where u_j is the point where $B_j = 1$,

$$\Theta = [u_1 u_2 \ldots u_m]^{\mathrm{T}} \tag{5}$$

And

$$\Gamma = [\prod_{i=1}^{n} A_i^1(x_i) \prod_{i=1}^{n} A_i^2(x_i) \ldots \prod_{i=1}^{n} A_i^m(x_i)]^{\mathrm{T}} \tag{6}$$

Finally, to realize the above Mamdani-type fuzzy control scheme, algorithm3 can show the coding process. Algorithm3 is the C8051F120DK code to deal with the Mamdani-type fuzzy control scheme.

In fact, choosing of the mean, m, and the variance, v, of Gaussian functions significantly affect the system performance. How to effectively select the best parameters will be an important link in the system response. If the system parameters are selected well, the performance of the platform will be better. If the selection of system parameters is not good, the system performance will not be good enough.

B. ON-LINE LEARNING ALGORITHM FOR FUZZY MECHANISM

To efficiently select the better parameters, based on the supervised gradient descent method, an on-line effective learning algorithm is used to modify the means and variances of the Gaussian functions in real-time. An adaptive Mamdani-like fuzzy controller is carried out as follows.

Here, the accurate system dynamics of the unicycle are absent; however, there is a proportional relationship between the angular acceleration of the vehicle and the input. When the system input is increasing (decreasing), the angular acceleration of the vehicle is increasing (decreasing) also. The architecture of the AMLFC control system is exhibited in Figure 9, where the reference signal d_m is given, and d is the vehicle slant angle. The cost function is defined as follows:

$$E = \frac{1}{2}(d_m - d)^2 = \frac{1}{2}e_m^2 \tag{7}$$

Algorithm 3 Fuzzy Control Algorithm

Input: Angle error ***E***, the change of rate of angle ***DE***, mean value of Gaussian function ***m***, variance value of Gaussian function ***sd***, fuzzy rule table ***t[5][5]***

Output: Desire fuzzy output for balance control ***U***

1. Limit the input variable into the interval between the largest mean value and the smallest mean value
2. See the input variables between which two mean value of Gaussian function, for example:
   if (((E>=m1)&&(E<=m2))&&((DE>=m6)&&(DE<=m7)))
   where *m1*, and *m2* are the mean value for *E*; *m6*, and *m7* are the mean value for *DE*, then its fire the x^{th} row, and y^{th} column of fuzzy rule table
3. Calculate the antecedent of fuzzy control algorithm, for example:

$$\begin{aligned} \boldsymbol{e1} &= exp(-pow((E - m1), 2)/pow(sd1, 2)); \\ \boldsymbol{e2} &= exp(-pow((m2 - E), 2)/pow(sd2, 2)); \\ \boldsymbol{de1} &= exp(-pow((DE - m6), 2)/pow(sd6, 2)); \\ \boldsymbol{de2} &= exp(-pow((m7 - DE), 2)/pow(sd7, 2)); \end{aligned}$$

   where *e1*, *e2* are the output of Gaussian function for *E*; *de1*, *de2* are the output of Gaussian function for *DE*
4. Calculate the output of fuzzy control algorithm by the center of gravity defuzzification as:

$$\begin{aligned} \boldsymbol{U} = {} & [(e1^*de1^*t[x][y]) + (e1^*de2^*t[x][y+1]) \\ & + (e2^*de1^*t[x+1][y]) + (e2^*de2^*t[x+1] \\ & \times [y+1])]/[(e1^*de1) + (e1^*de2) + (e2^*de1) \\ & + (e2^*de2)] \end{aligned}$$

End Algorithm

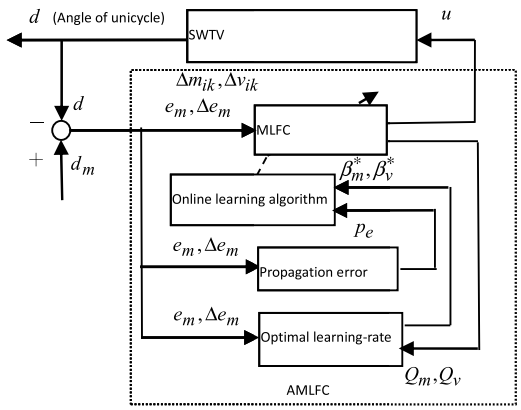

FIGURE 9. The control system block diagram.

where e_m is vehicle angle error. The propagation error term is given by

$$p_e = -\frac{\partial E}{\partial u} = -\frac{\partial E}{\partial e_m}\frac{\partial e_m}{\partial d}\frac{\partial d}{\partial u} = e_m\frac{\partial d}{\partial u}. \tag{8}$$

If the system mathematical model is always known, the system Jacobian term, $\partial d/\partial u$, can then be computed. If the system dynamics are absent, then $\partial d/\partial u$ cannot be calculated. Thus, the following equation can be used to approximate the system propagation error term [15]:

$$p_e \cong \Delta e_m + e_m \tag{9}$$

where Δe_m is the rate of change of the angle error. Moreover, on the basis of the gradient descent method, the adaptive laws for mean and variance, Δm and Δv, are derived as

$$\begin{aligned}\Delta m_{ik} &= -\beta_m \frac{\partial E}{\partial m_{ik}} = -\beta_m \frac{\partial E}{\partial u}\frac{\partial u}{\partial m_{ik}} \\ &= \beta_m p_e \frac{u_k - u}{\sum_{k=1}^{m}\prod_{i=1}^{n} A_i^k(x_i)} \prod_{i=1}^{n} A_i^k(x_i) \frac{2(x_i - m_{ik})}{v_{ik}^2} \end{aligned} \tag{10}$$

$$\begin{aligned}\Delta v_{ik} &= -\beta_v \frac{\partial E}{\partial v_{ik}} = -\beta_v \frac{\partial E}{\partial u}\frac{\partial u}{\partial v_{ik}} \\ &= \beta_v p_e \frac{u_k - u}{\sum_{k=1}^{m}\prod_{i=1}^{n} A_i^k(x_i)} \prod_{i=1}^{n} A_i^k(x_i) \frac{2(x_{ri} - m_{ik})^2}{v_{ik}^3} \end{aligned} \tag{11}$$

where the learning rates for the mean and variance are the positive factors β_m and β_v, respectively. The mean and variance of the discrete time N are revised as follows:

$$m_{ik}(N+1) = m_{ik}(N) + \Delta m_{ik}(N) \tag{12}$$

$$v_{ik}(N+1) = v_{ik}(N) + \Delta v_{ik}(N) \tag{13}$$

The adaptive laws of (12) and (13) ask for a good choice of the learning-rates β_m and β_v. For a small rate of learning-rates, it is easy to guarantee the convergence of system error; however, the speed of learning is slow. In contrast, if learning-rates are large, the system may become unstable. To train the fuzzy mechanism effectively, the variable learning-rates, which guarantee convergence of the system error, are derived. Algorithm4 is the C8051F120DK code to deal with on-line learning algorithm for the fuzzy mechanism.

C. CONVERGENCE ANALYSES

To ensure the convergence of the system error, the convergence analysis is proposed to derive the learning rates of the system parameters. To effectively train the AMLFC, the following adaptive learning rates can guarantee the system error convergence.

Theorem 1: Let $Q_s(N) = \partial u/\partial \mathbf{s}$ for $s = m$ and v, and let β_s be the learning rate for the system parameter of the AMLFC. The system tracking error converges if the learning rate, β_s, is chosen as

$$0 < \beta_s < \frac{2}{||Q_s(N)||^2 [1 + \Delta e_m(N)/e_m(N)]^2} \tag{14}$$

where $||\cdot||$ is the Euclidean norm.

Algorithm 4 Parameter Update Law

Input: Angle error ***E***, the change of rate of angle ***DE***, mean value of Gaussian function ***m***, variance value of Gaussian function ***sd***, fuzzy rule table *t[5][5]*, change of mean value ***dm***, change of variance value ***dsd***, learning rate of mean value ***beta_m***, learning rate of variance value ***beta_v***, the error term $p_e \cong \Delta e_m + e_m$

Output: Change of each updated parameter

1. See which fuzzy rule is fired in the fuzzy rule table, for example:
   if ((x==1)&&(y==1))
2. Calculate the change of mean value and variance value, for example:
   dm1=*beta_m*p_e*2*(t[x][y]−U)*(e1*de1) *((E−m1)/pow(sd1,2)) / [(e1*de1)+(e1*de2)+(e2*de1)+(e2*de2)]*
   dm2=*beta_m*p_e*2*(t[x+1][y]−U)*(e2*de1) *((E−m2)/pow(sd2,2)) / [(e1*de1)+(e1*de2)+(e2*de1)+(e2*de2)]*
   dm6=*beta_m*p_e*2*(t[x][y]−U)*(e1*de1) *((DE−m6)/pow(sd6,2)) / [(e1*de1)+(e1*de2)+(e2*de1)+(e2*de2)]*
   dm7=*beta_m*p_e*2*(t[x][y+1]−U)*(e1*de2) *((DE−m7)/pow(sd7,2)) / [(e1*de1)+(e1*de2)+(e2*de1)+(e2*de2)]*
   dsd1= *beta_v* ((E−m1)/sd1)*dm1/ beta_m;*
   dsd2= *beta_v* ((E−m2)/sd2)*dm2/ beta_m;*
   dsd6= *beta_v* ((DE−m6)/sd6)*dm6/ beta_m;*
   dsd7= *beta_v* ((DE−m7)/sd7)*dm7/ beta_m;*
3. Calculate the new mean value and variance value, for example:
   m1=m1+dm1;
   sd1=sd1+dsd1;

End Algorithm

Proof: Because $Q_s(N) = \frac{\partial u}{\partial s}$ for $s = m$ and v, the following is obtained:

$$\begin{aligned} Q_m(N) &= \frac{\partial u}{\partial \mathrm{m}} \\ &= \left[\frac{\partial u}{\partial m_{11}}, \cdots, \frac{\partial u}{\partial m_{n1}}, \cdots, \frac{\partial u}{\partial m_{1j}}, \cdots, \frac{\partial u}{\partial m_{ij}} \right. \\ &\quad \left. \cdots, \frac{\partial u}{\partial m_{nj}}, \cdots \frac{\partial u}{\partial m_{1m}}, \cdots, \frac{\partial u}{\partial m_{nm}}\right]^T \end{aligned} \tag{15}$$

and

$$Q_v(N) = \frac{\partial u}{\partial v} = \left[\frac{\partial u}{\partial v_{11}}, \cdots, \frac{\partial u}{\partial v_{n1}}, \cdots, \frac{\partial u}{\partial v_{1j}}, \cdots, \frac{\partial u}{\partial v_{ij}} , \cdots, \frac{\partial u}{\partial v_{nj}}, \cdots \frac{\partial u}{\partial v_{1m}}, \cdots, \frac{\partial u}{\partial v_{nm}}\right]. \tag{16}$$

A Lyapunov function is defined as

$$V(N) = \frac{1}{2} e_m^2(N) \tag{17}$$

then the change of the Lyapunov function is derived as

$$\Delta V(N) = V(N+1) - V(N) = \frac{1}{2}[e_m^2(N+1) - e_m^2(N)] \tag{18}$$

where $e_m(N+1)$ is represented by

$$e_m(N+1) = e_m(N) + \Delta e_m(N) = e_m(N) + \left[\frac{\partial e_m(N)}{\partial \mathbf{s}}\right]^T \Delta \mathbf{s} \tag{19}$$

Using (9), the following is obtained:

$$\frac{\partial e_m}{\partial \mathbf{s}} = \frac{\partial e_m}{\partial d}\frac{\partial d}{\partial u}\frac{\partial u}{\partial \mathbf{s}} = -\frac{p_e}{e_m(N)} Q_s(N) \tag{20}$$

Thus,

$$\begin{aligned} e_m(N+1) &= e_m(N) - \left[\frac{p_e}{e_m(N)} Q_s(N)\right]^T \beta_s p_e Q_s(N) \\ &= e_m(N)\left[1 - \beta_s \left(\frac{p_e}{e_m(N)}\right)^2 Q_s^T(N)\, Q_s(N)\right] \end{aligned} \tag{21}$$

From (18) and (21), $\Delta V(N)$ can be depicted as

$$\begin{aligned} \Delta V(N) = &\frac{1}{2}\beta_s p_e^2 ||Q_s(N)||^2 \\ &\cdot \left[\beta_s \left(\frac{\Delta e_m(N) + e_m(N)}{e_m(N)}\right)^2 ||Q_s(N)||^2 - 2\right] \end{aligned} \tag{22}$$

If β_s is chosen as $0 < \beta_s < \frac{2}{||Q_s(N)||^2[1+\Delta e_m(N)/e_m(N)]^2}$, then the value of $\Delta V(N)$ in (22) is negative. The system stability based on the Lyapunov analytical method is guaranteed. Therefore, the learning rate is adopted as $\frac{1}{||Q_s(N)||^2[1+\Delta e_m(N)/e_m(N)]^2}$ in this study.

According to Theorem 1, the learning rate parameters can be on-line adjusted automatically at each instant; thus, system error convergence is assured. Moreover, for system computing simplification and sensor precision, the learning-rate parameters of the AMLFC are not adjusted when $|e_m(N) + \Delta e_m(N)| < adj$, where adj is a selected small constant, and $|\cdot|$ is the absolute value symbol. Algorithm5 denotes the C8051F120DK code to deal with updating the learning rates of the system parameters. Fig. 9 is the control system block diagram. Fig. 10 is the program flow chart.

IV. SYSTEM RESPONSES

In this section, AMLFS is used to control the electric unicycle in real time. The goal of this experiment is to test the standing of the SWTV and allow it to move steadily in the passenger riding (the weight of the rider is approximately 100 kg). The states of the vehicle from the inclinometer and the gyro are used as inputs of the AMLFC. The inputs to AMLFC are the rate of change of the angle error and angle error of SWTV, respectively. Three cases, which are balance control, balance control for a given nonzero initial condition, and moving forward control, are presented here.

Algorithm 5 Learning Rate Update

Input: Angle error ***E***, the change of rate of angle ***DE***, mean value of Gaussian function ***m***, variance value of Gaussian function ***sd***, fuzzy rule table ***t[5][5]***, change of mean value ***dm***, change of variance value ***dsd***, learning rate of mean value ***beta_m***, learning rate of variance value ***beta_v***, the error term ***k=E+DE***

Output: Change of each updated learning rate value

1. Calculate the learning rate of mean value:
   beta_m=*1/((pow((1+((DE/E)),2))*(pow((1*dm1),2)+pow((1*dm2),2)+pow((1*dm3),2)+pow((1*dm4),2)+pow((1*dm5),2)+pow((1*dm6),2)+pow((1*dm7),2)+pow((1*dm8),2)+pow((1*dm9),2)+pow((1*dm10),2)))*
   where (*the parts of* **Algorithm4**)
   *dm1=beta_m**2*(t[x][y]-U)*(e1*de1) *((E-m1)/pow(sd1,2)) / [(e1*de1)+(e1*de2)+(e2*de1)+(e2*de2)]*
2. Calculate the learning rate of variance value:
   beta_sigma=*0.002/((pow((1+(DE/E)),2))*(pow(dsd1,2)+pow(dsd2,2)+pow(dsd3,2)+pow(dsd4,2)+pow(dsd5,2)+pow(dsd6,2)+pow(dsd7,2)+pow(dsd8,2)+pow(dsd9,2)+pow(dsd10,2)));*
   where (*the parts of* ***Algorithm4***)
   dsd1= *beta_v* ((E-m1)/sd1)*dm1/ beta_m;*

End Algorithm

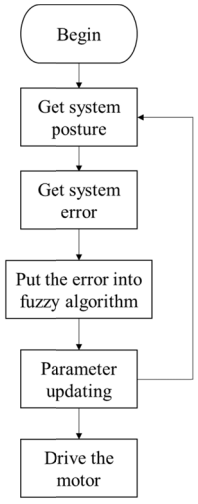

FIGURE 10. The program flow chart.

Fig. 11 shows the fuzzy membership functions. The inputs memberships, for which the linguistic values are positive big (PB), positive small (PS), zero (ZO), negative small (NS) and negative big (NB), are shown in Figs. 11.(a), (b), and the output membership function, for which the linguistic values are PB, PS, ZO, NS and NB, are shown in Fig. 11.(c). Table 1 shows the fuzzy rule table for the fuzzy controller. Moreover, the learning rates selected are $\beta_m = \beta_v = 0.02$ and adj is 0.1 in this work.

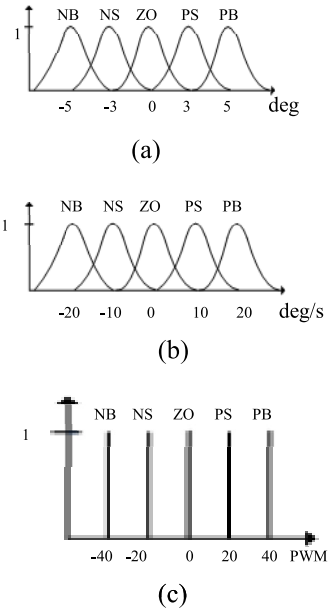

FIGURE 11. Fuzzy membership functions of the proposed controller.

TABLE 1. Fuzzy controller rule base.

	NB	**NS**	**ZO**	**PS**	**PB**
NB	NB	NB	NS	NS	ZO
NS	NB	NS	NS	ZO	PS
ZO	NS	NS	ZO	PS	PS
PS	NS	ZO	PS	PS	PB
PB	ZO	PS	PS	PB	PB

FIGURE 12. Experimental testing system.

For example, the antecedent part of the Gaussian membership function, where the linguistic value is positive big, can be represented as $\exp[-(x-5)^2/0.02^2]$ for angle error and $\exp[-(x-20)^2/0.02^2]$ for the rate of change of the angle error, respectively. Moreover, the consequent part of the fuzzy membership function, where the linguistic value is positive small, can be represented as $u_j = 20$ Newton. The SWTV real world control system is shown in Fig. 12.

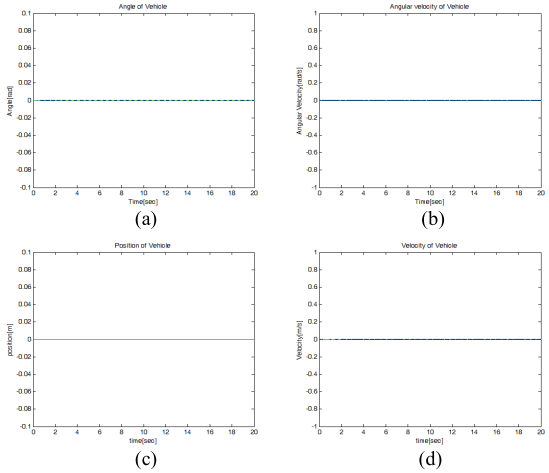

FIGURE 13. The system simulation response of the SWTV standing upright control. (a) The angle of SWTV. (b) The angular velocity of the SWTV. (c) The position of SWTV. (d) The velocity of the SWTV.

A. SEVERAL SIMULATION RESULTS

1) BALANCE CONTROL

In this case, a standing upright balance control at the original point is tested, and its target angle of SWTV is 0 degrees to ensure that a passenger who is riding on the SWTV rides stably. First, the fuzzy control system shown in (4) is considered. Automatic adjustment rules are shown in (12), (13) and Theorem 1. The system performance is shown in Fig. 13. The angle of the SWTV and the angular velocity of the SWTV are shown in Fig. 13(a) and Fig. 13(b), respectively. Moreover, the position of the SWTV and the velocity of the SWTV are shown in Fig. 13(c) and Fig. 13(d), respectively. Clearly, the vehicle can stand upright stably at the original point.

2) BALANCE CONTROL FOR NONZERO INITIAL CONDITIONS

Fig. 14 shows the control response of the SWTV under proposed AMLFC for nonzero initial conditions. In this simulation case, the SWTV is at approximately 15 degrees. The SWTV starts with a 15-degree slant angle. The body angle of the vehicle is shown in Fig. 14(a). Fig. 14(b) shows the angular velocity trajectory of the unicycle system. Moreover, the position of the SWTV and the velocity of the SWTV are shown in Fig. 14(c) and Fig. 14(d), respectively. In Fig. 14(a), the unicycle system is clearly returned from 15 degrees to the equilibrium position at approximately 1 second. At the same time, the angular velocity converges rapidly to zero. Clearly, the AMLFC control system can address the nonzero initial conditions.

3) MOVING FORWARD CONTROL

In this case, the vehicle moves forward to an intended target position. Here, the target position is approximately 100 cm away. The vehicle control performance is shown in Fig. 15. Fig. 15(a) shows the body angle response of the SWTV. Clearly, the system is in the forward state in the first 10 seconds. After 10 seconds, the system returns to its upright

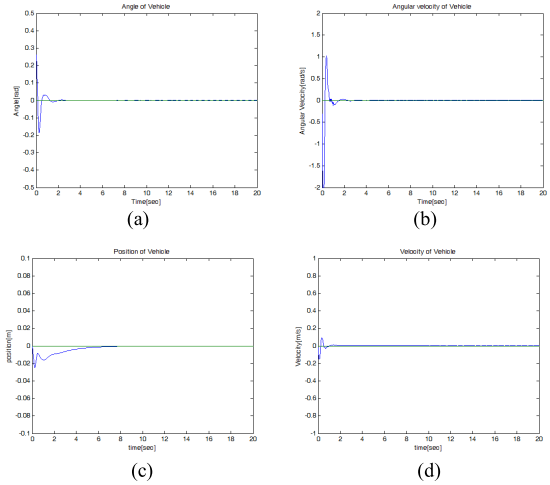

FIGURE 14. The system simulation response of the SWTV for nonzero initial conditions (approximately 15 degrees) (a) The angle of SWTV. (b) The angular velocity of the SWTV. (c) The position of SWTV. (d) The velocity of the SWTV.

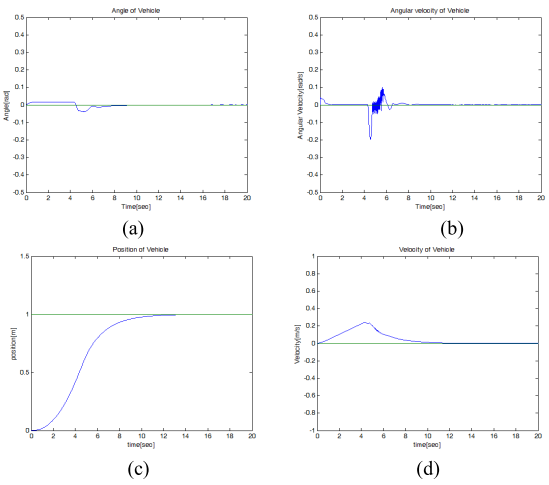

FIGURE 15. The system simulation response of the SWTV for moving forward (approximately 1 meter) (a) The angle of SWTV. (b) The angular velocity of the SWTV. (c) The position of SWTV. (d) The velocity of the SWTV.

balance condition. Fig. 15(c) shows the unicycle position trajectory. It is very clear that the system moves forward in 0 to 10 seconds. Then, the SWTV stops at 1 meter ahead of the origin. The angular velocity of the SWTV is shown in Fig. 15(b). Moreover, the velocity of the SWTV is shown in Fig. 15(d).

4) THE EFFECT OF PARAMETER UNCERTAINTIES ON THE DYNAMIC RESPONSE

In this case, the moving forward control is done again. However, at 10 seconds, the mean and the variance of the antecedent part of the Gaussian membership function, where the linguistic value is negative big, are set to zero for angle error and the rate of change of the angle error, respectively. The vehicle response is shown in Fig. 16. Comparing Fig. 15 with Fig. 16, the difference is small. The biggest difference is shown in Fig. 16(c). Fig. 16(c) is above the target position during 12 to 18 seconds. However, the position trajectory finally converges to the intended target position. In this case, the proposed controller can deal successfully with the effect of parameter uncertainties.

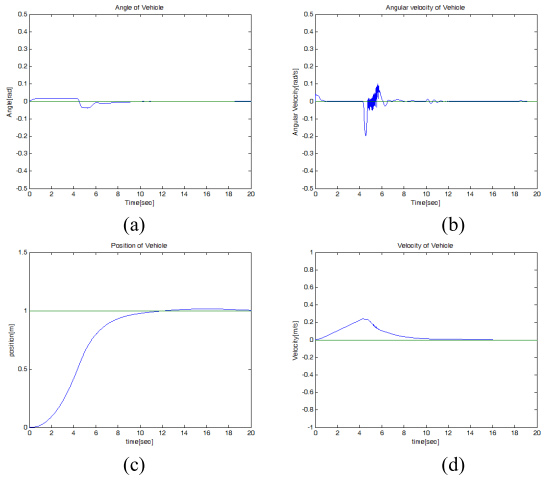

FIGURE 16. The system simulation response of the SWTV for effect of parameter uncertainties (a) The angle of SWTV. (b) The angular velocity of the SWTV. (c) The position of SWTV. (d) The velocity of the SWTV.

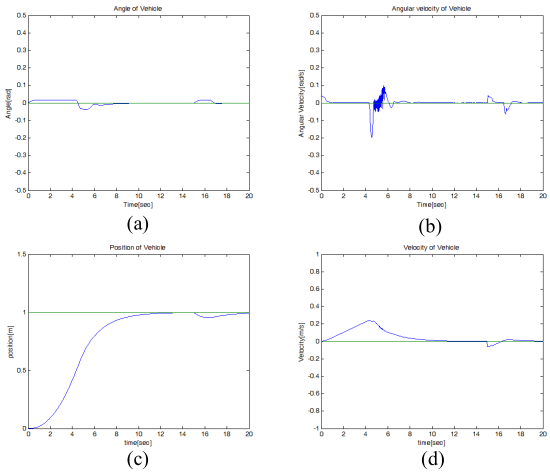

FIGURE 17. The system simulation response of the SWTV for testifying to the robustness of the proposed control scheme (a) The angle of SWTV. (b) The angular velocity of the SWTV. (c) The position of SWTV. (d) The velocity of the SWTV.

5) TESTIFYING TO THE ROBUSTNESS OF THE PROPOSED CONTROL SCHEME

In this case, the moving forward control is still used to test system robustness. However, an extra force, 500 Newtons, is added to system at 15 seconds. The vehicle response is shown in Fig. 17. Comparing Fig. 15 with Fig. 17, the difference appears in 15 to 20 seconds. Nevertheless, the trajectories converge quickly. In this case, the robustness of the proposed control scheme is conformed.

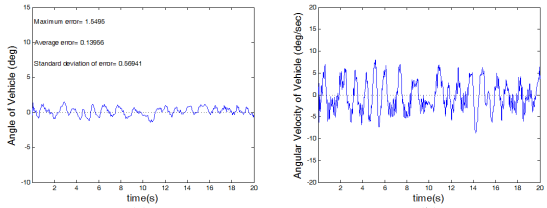

FIGURE 18. The system experiment response of the SWTV standing upright control. (a) The angle of SWTV. (b) The angular velocity of the SWTV.

B. SEVERAL EXPERIMENTAL RESULTS

1) BALANCE CONTROL

In this subsection, a passenger is riding on the SWTV to test the ability of the vehicle to stand upright stably. Moreover, in this case, SWTV can also stand up self-balanced when a person rides on it without touching the ground. The system performance is shown in Fig. 18. The angle of the SWTV and the angular velocity of the SWTV are shown in Fig. 18(a) and Fig. 18(b), respectively. The angle of the vehicle is found to be in the interval between -1 degrees and $+2$ degrees. Moreover, the angular velocity is also maintained within a certain range between -10 degrees/sec and $+10$ degrees/sec. Clearly, the vehicle can stand upright stably.

For comparison, the classical PID, the adaptive fuzzy sliding mode control (AFSMC) [16], and the Mamdani-like fuzzy control method are used to control the SWV. In the Mamdani-like fuzzy controller, the Gaussian function is used as the membership function of the antecedent part. The consequent part is singleton. The chosen parameters of the classical PID controller are: $k_p = 0.2$, $k_i = 0.1$ and $k_d = 0.2$. The parameters of the AFSMC method are: $\gamma_f = 0.3$, $\gamma_g = 0.2$, $\gamma_k = 0.001c_1 = 10$, $g_{\max} = 1.46$, $g_{\min} = 0.74$, $F = 16$. Moreover, the normalization factor of the fuzzy control term is $k_{afs} = 5$. In this case, a balance control is considered, and its object angle of SWV is 0 degrees to keep a passenger who is riding on the SWV riding stably. Fig. 19 is the system response. Figures 19(a), 19(b), 19(c), 19(d), 19(e), and 19(f) show the comparison results for the fuzzy control, the classical PID, and the AFSMC, respectively. Based on the proposed control system, the angle of the SWTV and the angular velocity of the SWTV are shown in Fig. 18(a) and Fig. 18(b), respectively. The angle of the vehicle is in the interval between -1 degrees and $+2$ degrees. Clearly, the vehicle can stand upright stably, and the system responses in Fig. 18(a) are better than those in the other figures. These results show that the tracking error of the AMLFC converges faster than the tracking error of the other methods. It is obvious that favorable tracking responses can be obtained by the proposed scheme.

2) BALANCE CONTROL FOR NONZERO INITIAL CONDITIONS

Fig. 20 shows the experiment response of the SWTV with nonzero initial conditions. In this experimental case, the unicycle is started at approximately 5 degrees. The rider slants the SWTV forward at 5 degrees. The body angle of the vehicle

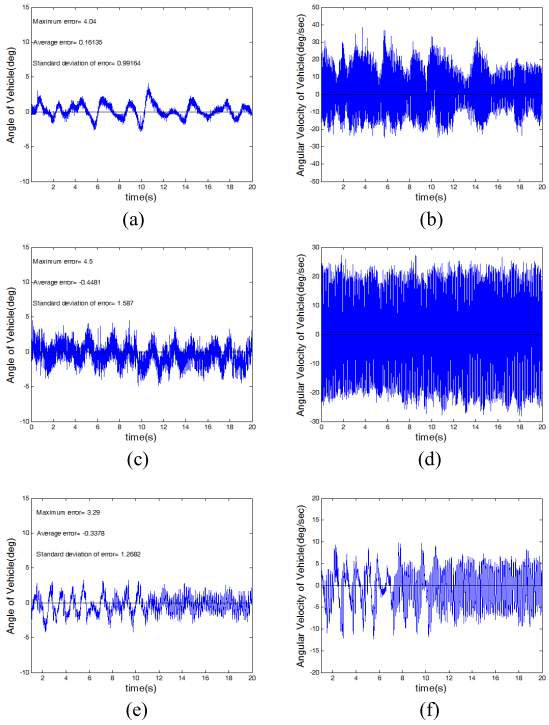

FIGURE 19. The system performance of the SWTV balance control. (a) The angle of SWTV for fuzzy control. (b) The angular velocity of the SWTV for fuzzy control. (c) The angle of SWTV for PID control. (d) The angular velocity of the SWTV for PID control. (e) The angle of SWTV for AFSMC. (f) The angular velocity of the SWTV for AFSMC.

is shown in Fig. 20(a). Fig. 20(b) shows the angular velocity trajectory of the unicycle system. In Fig. 20(a), the unicycle system clearly is returned from 5 degrees to the equilibrium position quickly. Moreover, the angular velocity converges rapidly also. Clearly, the AMLFC control system can deal with the nonzero initial conditions. Figures 20(c) and 20(d) are the body angle and angular velocity of SWTV based on fuzzy control. Figures 20(e) and 20(f) are the body angle and angular velocity of SWTV under PID control. Figures 20(g) and 20(h) are the body angle and angular velocity of SWV based on AFSMC. Experimental results indicate that good control performance is achieved by the proposed AMLFC.

3) MOVING FORWARD CONTROL

In this test, an expected target is given, and then the vehicle moves forward to the target position. Here, the target position is approximately 100 cm away. The vehicle system response is shown in Fig. 21. Fig. 21(a) shows the system angle response of the SWTV. Clearly, the system is in the forward state in the first 6 seconds of the experiment. After 6 seconds, the system returns to its upright balance condition. Fig. 21(b) shows the unicycle position trajectory. It is very clear that the system moves forward in 0 to 6 seconds. Then, the unicycle stops at approximately 1 meter ahead of the origin. The SWTV can stand upright in the target position in 6 to 20 seconds, when the person above does not touch

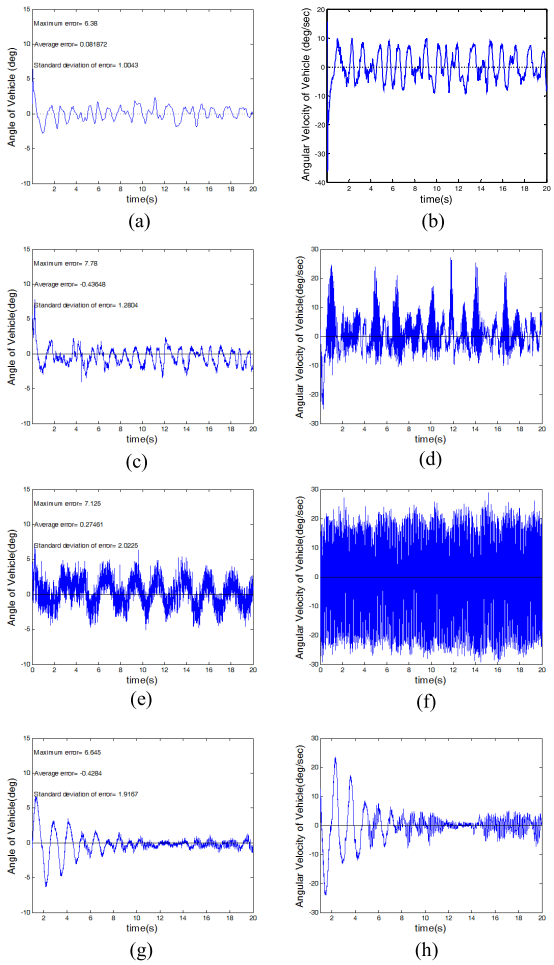

FIGURE 20. The system experimental response of the SWTV for nonzero initial conditions (approximately 5 degrees). (a) The body angle of the SWTV for AMLFC. (b) The angular velocity of the SWTV for AMLFC. (c) The angle of SWTV for fuzzy control. (d) The angular velocity of the SWTV for fuzzy control. (e) The angle of SWTV for PID control. (f) The angular velocity of the SWTV for PID control. (g) The angle of SWTV for AFSMC. (h) The angular velocity of the SWTV for AFSMC.

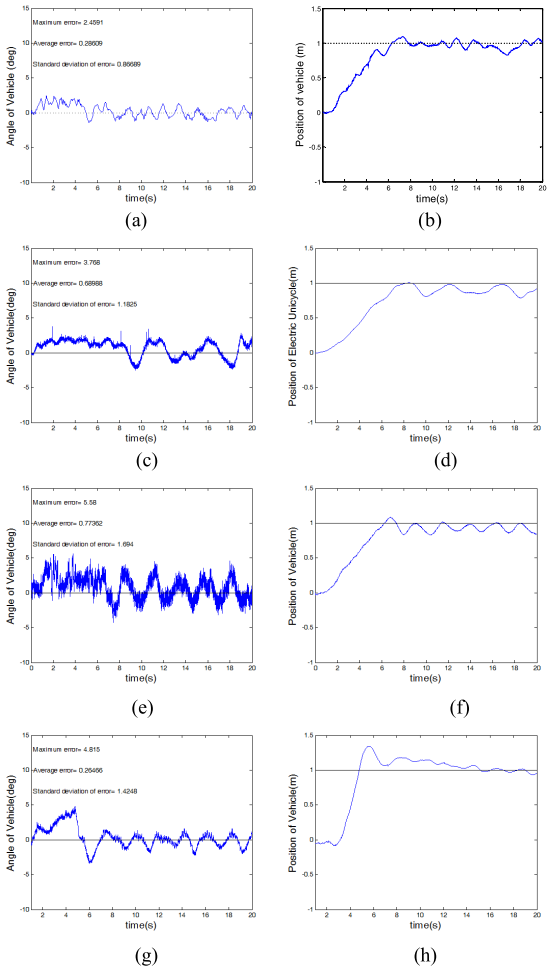

FIGURE 21. The system performance of the SWTV is commanded to move forward. (a) The body angle of the SWTV for AMLFC. (b) The angular velocity of the SWTV for AMLFC. (c) The angle of SWTV for fuzzy control. (d) The angular velocity of the SWTV for fuzzy control. (e) The angle of SWTV for PID control. (f) The angular velocity of the SWTV for PID control. (g) The angle of SWTV for AFSMC. (h) The angular velocity of the SWTV for AFSMC.

the ground. Figures 21(c), 21(d), 21(e), 21(f), 21(g) and 21(h) show the experimental results for the fuzzy control, the classical PID, and the AFSMC, respectively. These results show that the tracking error of the AMLFC converges faster than the tracking error of the other methods. The passenger chatter is reduced quickly because of the advantages of the AMLFC. Clearly, the AMLFC is superior to the others in capturing the system uncertainties for an unmodeled system.

For recording respective control performances, the root-mean-square-error (RMSE) [13] for the angle tracking errors is defined as:

$$RMSE = \sqrt{\frac{1}{N}\sum_{i=1}^{N} e_{\theta}^{2}(i)} \tag{23}$$

where $N = 4000$ is sampling times for the angle tracking errors. The unit of $RMSE$ is degrees. The experimental performance comparisons of the classical PID, the fuzzy control method, AFSMC, and AMLFC scheme are summarized in Table 2.

TABLE 2. Performance comparisons.

Performance / Control condition	AMLFC	Fuzzy control	PID	ASMCF
Balance control	0.5863	1.0047	1.6490	1.3124
Balance control with nonzero initial condition	1.0076	1.3528	2.0411	1.4492
Moving forward control	0.9129	1.3690	1.8623	1.9640

According to the RMSE measures in Table 2, the proposed AMLFC scheme has the minimum root-mean-square-error.

Based on the above experimental results and Table 2, the AMLFC control system can achieve good control performance for SWTV rather than the other methods. The proposed controller is suitable for SWTV real-time control. Fig. 22 is a sequence of the experimental photographs.

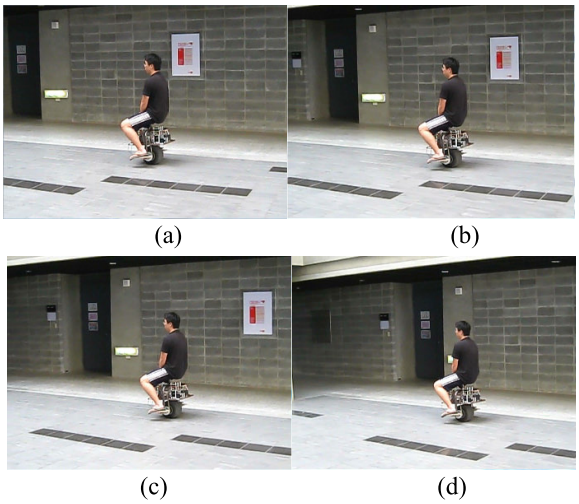

FIGURE 22. The sequence of experiments.

V. CONCLUSION

In this work, the mechanical structure design of the single-wheel transportation vehicle (SWTV) was completed first, and the handmade circuits, control boards and the driving device were also integrated simultaneously. Moreover, this study involved the successful implementation of an SWTV based on a novel adaptive Mamdani-like fuzzy control system. The experimental results demonstrated the usefulness of the proposed handmade circuits and control system. The major results of this work include: (1) the successful design and implementation of an SWTV hardware, and (2) the successful realization of the proposed AMLFC control scheme to control the SWTV that a person is riding on. Moreover, an SWTV can also stand up in a fixed-point self-balance without touching the ground when a person rides on it.

REFERENCES

[1] M. Yue, C. An, and Z. Li, "Constrained adaptive robust trajectory tracking for WIP vehicles using model predictive control and extended state observer," *IEEE Trans. Syst., Man, Cybern. Syst.*, vol. 48, no. 5, pp. 733–742, May 2018.

[2] X. Yang and X. Zheng, "Swing-up and stabilization control design for an underactuated rotary inverted pendulum system: Theory and experiments," *IEEE Trans. Ind. Electron.*, vol. 65, no. 9, pp. 7229–7238, Sep. 2018.

[3] C. A. Ibanez, J. C. M. Garcia, A. S. Lopez, J. J. Rubio, and M. S. S. Castanon, "Stabilization of the inverted cart-pendulum system with linear friction," *IEEE Latin Amer. Trans.*, vol. 16, no. 6, pp. 1650–1657, Jun. 2018.

[4] H. O. Erkol, "Optimal PIλDμ controller design for two wheeled inverted pendulum," *IEEE ACCESS*, vol. 6, pp. 75709–75717, 2018.

[5] M. V. Basin, P. C. R. Ramirez, and F. Guerra-Avellaneda, "Continuous fixed-time controller design for mechatronic systems with incomplete measurements," *IEEE/ASME Trans. Mechatronics*, vol. 23, no. 1, pp. 57–67, Feb. 2018.

[6] H.-G. Han, X.-L. Wu, Z. Liu, and J.-F. Qiao, "Design of self-organizing intelligent controller using fuzzy neural network," *IEEE Trans. Fuzzy Syst.*, vol. 26, no. 5, pp. 3097–3111, Oct. 2018.

[7] J. Huang, M. Ri, D. Wu, and S. Ri, "Interval type-2 fuzzy logic modeling and control of a mobile two-wheeled inverted pendulum," *IEEE Trans. Fuzzy Syst.*, vol. 26, no. 4, pp. 2030–2038, Aug. 2018.

[8] D. Wang, H. He, and D. Liu, "Intelligent optimal control with critic learning for a nonlinear overhead crane system," *IEEE Trans. Ind. Informat.*, vol. 14, no. 7, pp. 2932–2940, Jul. 2018.

[9] J. Wu, Z.-G. Wu, J. Li, G. Wang, H. Zhao, and W. Chen, "Practical adaptive fuzzy control of nonlinear pure-feedback systems with quantized nonlinearity input," *IEEE Trans. Syst., Man, Cybern. Syst.*, vol. 49, no. 3, pp. 638–648, Mar. 2019.

[10] Y. Sheng, F. L. Lewis, and Z. Zeng, "Exponential stabilization of fuzzy memristive neural networks with hybrid unbounded time-varying delays," *IEEE Trans. Neural Netw. Learn. Syst.*, vol. 30, no. 3, pp. 739–750, Mar. 2019.

[11] J. Yu, J. Liu, Z. Wu, and H. Fang, "Depth control of a bioinspired robotic dolphin based on sliding-mode fuzzy control method," *IEEE Trans. Ind. Electron.*, vol. 65, no. 3, pp. 2429–2438, Mar. 2018.

[12] J. Xu, Z. Hou, W. Wang, B. Xu, K. Zhang, and K. Chen, "Feedback deep deterministic policy gradient with fuzzy reward for robotic multiple peg-in-hole assembly tasks," *IEEE Trans. Ind. Informat.*, vol. 15, no. 3, pp. 1658–1667, Jul. 2019.

[13] C.-H. Chiu and W.-J. Wang, "Implementation of a ball inverted pendulum with omnidirectional moving ability using a robust fuzzy control strategy," *ISA Trans.*, vol. 89, pp. 287–298, Mar. 2019.

[14] Y. Wang, Y. Xia, C. K. Ahn, and Y. Zhu, "Exponential stabilization of Takagi–Sugeno fuzzy systems with aperiodic sampling: An aperiodic adaptive event-triggered method," *IEEE Trans. Syst., Man, Cybern. Syst.*, vol. 49, no. 2, pp. 444–454, Feb. 2019.

[15] C.-M. Lin and Y.-F. Peng, "Adaptive CMAC-based supervisory control for uncertain nonlinear systems," *IEEE Trans. Syst., Man, Cybern. B, Cybern.*, vol. 34, no. 2, pp. 1248–1260, Apr. 2004.

[16] M. Roopaei, M. Zolghadri, and S. Meshksar, "Enhanced adaptive fuzzy sliding mode control for uncertain nonlinear systems," *Commun. Nonlinear Sci. Numer. Simul.*, vol. 14, nos. 9–10, pp. 3670–3681, Sep. 2009.

CHIH-HUI CHIU was born in Taiwan. He received the B.S. degree in electrical engineering from the Tatung Institute of Technology, Taipei, Taiwan, in 1994, and the M.S. and Ph.D. degrees in electrical engineering from National Central University, Taiwan, in 1996 and 2000, respectively.

He is currently a Professor with the Department of Communications, Navigation, and Control Engineering, National Taiwan Ocean University, Keelung City, Taiwan. His research interests include fuzzy logic theory, intelligent control, robot, and control theory applications.